Accepted Manuscript

Research paper

Investigating the structural, morphological, dielectric and electric properties of the multiferroic $(La_{0.8}Ca_{0.2})_{0.9}Bi_{0.1}FeO_3$ material

H. Issaoui, A. Benali, M. Bejar, E. Dhahri, M.P.F. Graca, M.A. Valente, B.F.O. Costa

PII: S0009-2614(19)30559-7
DOI: https://doi.org/10.1016/j.cplett.2019.07.016
Reference: CPLETT 36588

To appear in: *Chemical Physics Letters*

Received Date: 31 May 2019
Revised Date: 1 July 2019
Accepted Date: 6 July 2019

Please cite this article as: H. Issaoui, A. Benali, M. Bejar, E. Dhahri, M.P.F. Graca, M.A. Valente, B.F.O. Costa, Investigating the structural, morphological, dielectric and electric properties of the multiferroic $(La_{0.8}Ca_{0.2})_{0.9}Bi_{0.1}FeO_3$ material, *Chemical Physics Letters* (2019), doi: https://doi.org/10.1016/j.cplett.2019.07.016

Investigating the structural, morphological, dielectric and electric properties of the multiferroic $(La_{0.8}Ca_{0.2})_{0.9}Bi_{0.1}FeO_3$ material

H. Issaoui[1,3*], A. Benali [1,2], M. Bejar[1], E. Dhahri[1], M.P.F. Graca[2], M.A. Valente[2], B.F.O. Costa[3]

[1] Laboratoire de Physique Appliquée, Faculté des Sciences, Université de Sfax, B.P. 1171, 3000 Sfax, Tunisie.

[2] I3N and Physics Department, University of Aveiro, 3810-193, Aveiro, Portugal.

[3] CFisUC, Physics Department, Universityof Coimbra, Rua Larga, P-3004-516 Coimbra, Portugal.

ABSTRACT

The $(La_{0.8}Ca_{0.2})_{0.9}Bi_{0.1}FeO_3$ (LCBFO) compound has been synthesized by the sol-gel method and characterized by X-Ray Diffraction (XRD), Scanning Electron Microscope (SEM), Raman spectroscopy and electrical impedance spectrometry. XRD results revealed that $(La_{0.8}Ca_{0.2})_{0.9}Bi_{0.1}FeO_3$ crystals are orthorhombic, belonging to the *Pnma* space group. The SEM measurements showed that the sample presents a large distribution of nano-grains connected to each other. The relaxation process and the electrical conductivity are awarded to the same type of charge carriers characterized by similar values of the activation energy determined from loss factor tangent $tg(\delta)$, the imaginary part of the permittivity and from the Modulus spectrum. The *ac*-conductivity was analysed to examine the conduction mechanism, using the Jonscher's universal power-law given by: $\sigma_{ac}(\omega) = \sigma_{dc} + A\omega^s$. Based on the parameter *s* behavior, the conductivity was studied according to the NSPT model (non-overlapping small polaron tunneling).

***Keywords*:** multiferroic/ Sol-gel/ dielectric/ *ac*-conductivity/ Permittivity.

I. INTRODUCTION

Perovskite ferrites with general formula $AFeO_3$ are one of the most promising materials for several application areas. Recently, they have been used for solid oxide fuel cells, sensors, magnetic memories, spintronic devices, *etc.*. **[1-5]**.

Besides, it was proven that $LaFeO_3$ compound is a multiferroic material at room temperature with a weak coupling between the electric and magnetic orderings **[6]**.

The $(La_{1-x}A_x)(Fe_{1-y}B_y)O_3$ compounds (A = *Ba, Ca, Pb, Sr*/ B = *Cr, Sm, Nb*..) have been widely studied by combining the substitution and the preparation method effects

in order to enhance the dielectric, ferromagnetic and ferroelectric properties **[7-9]**. Furthermore, these materials presented a giant dielectric constant and low dielectric loss at around room temperature **[7].** Materials with high dielectric permittivity are used to manufacture electronic devices especially as Capacitors and Dynamic Random Access Memory (DRAM) **[10-12]**.

The Ca-doped $LaFeO_3$ materials were used as solid oxide fuel cell cathode (SOFC) and as gas sensors **[13-18]**. In our preceding study, the relaxation process in the $La_{0.8}Ca_{0.2}FeO_3$ compound was found to be a polaronic one with the hopping motions of charge carrier between iron ions **[19]**. The non-overlapping small polaron tunnelling (NSPT) model was used to study the conduction mechanism for this compound.

Moreover, it was reported that the introduction of the diamagnetic bismuth element enhances the ferromagnetic and ferroelectric properties **[20, 21]**. In another previous work, we have proven that the simultaneous substitution of lanthanum and calcium ions by the bismuth ones in $(La_{0.8}Ca_{0.2})_{1-x}Bi_xFeO_3$ compounds sintered at 900 °C, did not affect the crystallinity structure with an enhancement of the magnetization. This is thanks to the increase of the Fe^{3+} ions with the introduction of Bi^{3+} ions in A-site, which directly increases the ferromagnetic Fe^{3+}-Fe^{3+} interactions **[22]**. Besides, it was reported that a 10% concentration of bismuth ions presents a critical value above where the unit cell volume changes its behavior to decrease after increasing below this concentration value **[23]**. Also, it was found that the $La_{0.9}Bi_{0.1}FeO_3$ compound presents the highest saturated magnetization value with smallest crystallite size value."

According to the previous purposes, we studied in this work the effect of insertion of 10 % of Bismuth ion in the A-site of the $La_{0.8}Ca_{0.2}FeO_3$ compound on the structural, morphological, dielectric and electric properties.

II. EXPERIMENTAL DETAILS

II.1. Synthesis

The ferrite sample $(La_{0.8}Ca_{0.2})_{0.9}Bi_{0.1}FeO_3$ (LCBFO) was prepared by the sol–gel method **[24, 25]** using as raw materials lanthanum nitrate$\left(La(NO_3)_3 6H_2O\right)$, bismuth nitrate $\left(Bi(NO_3)_3 5H_2O\right)$, calcium nitrate $\left(Ca(NO_3)_3 4H_2O\right)$, ferric nitrate

$(Fe(NO_3)_3 9H_2O)$ and citric acid (all *pro-analysis* purity) according to the following reaction equation:

$$0.72 \times La(NO_3)_3 + 0.18 \times Ca(NO_3)_2 + 0.10 \times Bi(NO_3)_3 + Fe(NO_3)_3 \rightarrow (La_{0.8}Ca_{0.2})_{0.9}Bi_{0.1}FeO_3$$

In a first step, according to this reaction equation, we have dissolved the adequate amount of each initial nitrate precursor in an ion free water. Afterwards, citric acid, used as a metal chelating agent, was added to the mixture in a molar ratio n (Metal ions): n (citric acid) = 1:2. Then, the polyethylene glycol was added to the mixture, which was maintained under constant stirring, for almost 2 hours until the formation of a viscous gel. The resulting gel was then heated to 170 °C until a black powder was formed. For subsequent annealing, the samples were placed in an electric oven at 300 °C, for 12 hours. Then, the powder was pressed into thin pellets, of about 12 mm in diameter and 1.5 mm in thickness, and subjected to heat treatments at different temperatures (400 and 600 °C for 12 hours), interrupted by grinding cycles. Finally, the obtained powder was heated at 800 °C for 4 hours.

II.2. Apparatus

The phase purity, homogeneity, lattice structure and cell parameters of the synthesized compound were obtained by X-Ray Diffraction (XRD) analysis, using a Bruker 8D Advance X-ray powder diffractometer, with Cu-Kα_1 radiation $(\lambda = 1.5406\ \text{Å})$, in the θ–2θ Bragg-Brentano geometry. The acquisition was in the 2θ range of 5-90°, with a step of 0.02° and an acquisition time for each step of 1 s. The XRD data were also used for obtaining the lattice parameters by means of Rietveld analysis **[26]**, using the FULLPROOF program. Microstructures and grain sizes were observed by a TESCAN VEGA3 SBH microscope, operating at 20 kV and equipped with an EDS detector BrukerXFlagh 410M, which allowed the detection of the characteristic X-rays emitted by the sample and, consequently, the identification of its chemical elements. For the analysis, a little amount of the compound powder was deposited on a carbon tape.

The dielectric measurements were performed in air atmosphere using an electric furnace equipped with a Eurotherm 3508 controller. For these measurements, a Network Analyzer Agilent 4294, operating between 100 Hz and 1 MHz in the C_p-R_p configuration (capacitance in parallel with resistance) was used **[27]**. The *ac* impedance of the sample was measured between 110 and 330 K. During the

measurement, the pre-heated pellet was mechanically pressed between two parallel platinum plates working as electrodes.

III. RESULTS AND DISCUSSION

III.1. Structural properties

The performed Rietveld refinement of the XRD data **(Fig. 1)** revealed that the studied compound crystallizes in an orthorhombic structure with the *Pnma* space group (*a* = 5.513(6) Å; *b* = 7.797(2) Å; *c* = 5.527(6) Å).

The crystallite size of the prepared compound was calculated by basing ourselves on the XRD results with the Scherer formula and the Halder-Wagner (H-W) method. The average crystallites size D_{SC} was calculated according to the following Scherer formula **[28]**:

$$D_{SC} = \frac{0.9 \times \lambda}{\beta \times cos\theta} \qquad \textbf{Eq. (1)}$$

Where λ is the used wavelength, θ is the Bragg angle for the most intense peak, and β is the half-height-width of this peak. The calculated D_{SC} value was found to be equal to 36.4 *nm*, which confirmed the nanosize nature of the obtained crystallites.

The Halder-Wagner (H-W) method is another method for determining the crystallites size using the following equation:

$$\left(\frac{\beta^{*}_{hkl}}{d}\right)^2 = \frac{1}{D_{WH}}\left(\frac{\beta^{*}_{hkl}}{d^{*2}_{hkl}}\right) + \left(\frac{\varepsilon}{2}\right)^2 \qquad \textbf{Eq. (2)}$$

where: $\beta^{*}_{hkl} = \frac{\beta_{hkl}\, cos\theta}{\lambda}$, $d^{*}_{hkl} = \frac{2\, sin\theta}{\lambda}$ and ε is a coefficient related to the effect of stress on the crystallites.

Afterwards, by the representation of $\left(\frac{\beta^{*}_{hkl}}{d}\right)^2$ as a function of $\left(\frac{\beta^{*}_{hkl}}{d^{*2}_{hkl}}\right)$ **(Fig. 2)**, we can determine the crystallites size (D_{WH}) and the microstrain (ε), respectively, from the inverse of the slope of the linearly fitted data and from the intercept of the line. The (D_{WH}) and (ε) values are found to be equal to 44.8 *nm* and 1.2 x10^{-5}, respectively. It is clear that the calculated crystallites size value using the Halder-Wagner method is slightly higher than that calculated by the Debye Scherrer formula. This difference could be explained by the fact that the Scherrer's formula does not take into account strain contribution to the X-ray line broadening.

It is important to mention that porosity is one of the key parameters to understand the electrical and dielectric properties. This parameter was calculated using the following equation **[29]**:

$$p(\%) = 1 - \frac{d}{d_x} \quad \textbf{Eq. (3)}$$

where d_x is X-Ray Density ($d_x = M/N_A.a^3$) **[29]**, while d is the bulk density.
The porosity of the prepared compound was found to be around 48,444 %. This value is in a good agreement with previous works **[30, 31]**.

III.2. Morphological study

We exposed the TEM image of the prepared LCBFO compound in **Fig. 3(*a*)**, which showed a relatively uniform distribution, confirming that the sol-gel method is a good process for preparing uniform and dense powders. We also noticed that all particles were found to be nearly spherical. In order to confirm the purity of the synthesized material, EDX analysis was undertaken **(Fig. 3(*b*))**. The peaks revealed the presence of La, Ca, Bi and Fe elements, which confirms that they are all non-volatile and that there is no loss of any integrated element after sintering.

The average grains size, obtained from an automatic statistical count of particle size performed on SEM image using the Image-J software, was found to be around (43.7 ±7.2) nm (**Fig. 3(*c*)**). It is clear that SEM gives an average value 6.6 times bigger than the average one determined by X-ray diffraction diagrams and 5.3 times bigger than the average value established from the Halder-Wagner method. This discrepancy confirmed that each grain is formed by several crystallites.

III.3 Dielectric study

Temperature and frequency dependence of the dielectric constant (ε') and the dielectric loss $(tg\delta)$ were recorded in the temperature range between 110 and 330 K and the frequency from 5 kHz to 1 MHz **(Fig. 4(a))**. We can note that when increasing temperature, ε' increases until a critical temperature (T_m), known as the transition temperature, and above which it decreases with further increase in temperature. This temperature is attributed to the first-order Ferroelectric-Paraelectric (FE-PE) phase transition. This transition was obtained in the same temperature range for pure and Cr-doped $GdFeO_3$ compounds **[32, 33]**, but at higher temperature for $LaFeO_3$ sample **[34]**. This behavior can be related to the thermal energy; the increase of temperature allows the electric dipoles to gain thermal energy and to be aligned with the applied

electric field, which increases the dielectric constant. Above T_m, the thermal energy is sufficiently large. So, the dipoles start to be randomly oriented and the sample becomes Paraelectric **[34]**. We can deduce that the insertion of both calcium and bismuth ions decreases the FE-PE phase transition temperature. Also, compared to the pure $LaFeO_3$ compound, the LCBFO sample presents a higher dielectric constant ($\varepsilon_{max}^{'}$ was around 600 at 715 K for LFO compound).

Fig. 4(*b*) showed the thermal variation of the dielectric loss ($tg\delta$) measured at different frequencies. It is seen that the appearance of a thermally activated relaxation peak, with an augmentation of its intensity when increasing frequency. The frequency dependence of the dielectric loss relaxation peak indicated a polaronic conduction relaxation mechanism as it was reported for pure and Ca-doped $LaFeO_3$ **[19]**.

Moreover, the dielectric constant showed an inflection point for each frequency at low temperatures accompanied by a peak in the corresponding dielectric tangent loss curve. The peak position (T_m) was found to obey the Arrhenius relation defined as follows:

$$f = f_0 \, exp\left(- \frac{E_a}{k_B \times T_m} \right) \qquad \textbf{Eq. (4)}$$

Where f_0, T_m, E_a and k_B have the known meanings. We plotted the $Ln(f)$ as the function of $\left(\frac{1}{T_m}\right)$ and fitted the curve according to the **Eq. (4)**. The Arrhenius curve, the extracted activation energy and the relaxation time values are shown in **Fig. 5**. The activation energy (E_a), obtained from the slope of the well fitted straight line, is found to be equal to 0.344 eV, which is slightly higher than that found for $La_{0.2}Ca_{0.2}FeO_3$ compound **[19]**. The relaxation time calculated from the intercept of the linear fitting of the Arrhenius plot $\left(\tau_0 = \frac{1}{2\pi f_0}\right)$, f_0= *exp*(*Intercept*) and found around 10^{-14} s. Both values are in a good agreement with literature **[19, 35, 36]** and confirmed that the dielectric process is related to the polaron dynamics.

Fig. 6 showed the frequency dependence of the imaginary part of the complex Modulus $(M^{''})$ measured at different temperatures. The appearance of two peaks for each temperature are clearly seen. Peaks with maximum values around 7×10^{-3}, shown in **Fig. 6(*a*)**, are attributed to the grains contribution while those with maximum values around 3×10^{-4} **(Fig. 6(*c*))** correspond to the boundary grains contribution.

One can see that all peaks shift to the high frequency region when increasing the temperature indicating a thermally activated relaxation mechanism. We have analysed the Modulus relaxation peaks for both contributions using the Arrhenius formula as shown in **Figs. 6(*b*)** and **(*d*)** for grains and boundary grains contributions, respectively. The activation energies for both contributions were found so close and equal to that obtained from the dielectric tangent loss.

III.4. *ac*-conductivity and conduction mechanism

In **Fig. 7** we plotted the variation of $Ln(\sigma_{ac}T)\ vs.\ (1000/T)$ recorded at certain frequencies (0.5, 1, 5, 10 and 50 kHz). Over the temperature range of 140 to 300 K, the *ac*-conductivity is characterized by two different regions, suggesting that electrical conduction occurs via two different processes. In the low temperature region $(R_1{:}T < 220\ K)$, the conductivity is not thermally activated in contrast to the behavior at the second region $(R_2{:}T \geq 220\ K)$ where the conductivity increases with increasing the temperature and show a frequency dependence. In the second region, we calculated the *ac*-conductivity activation energy, which was around 0.346 eV. This value is very close to those previously deduced from the dielectric tangent loss and the imaginary part of the Modulus, which suggests that both the conduction and the relaxation mechanisms are polaronic and are due to the electrons hopping between iron states (Fe^{2+} and Fe^{3+}).

In the first region, where the *ac*-conductivity is frequency independence, the conduction mechanism will be discussed according to the thermal variation of the Jonscher's power-low "s" parameter.

We plotted in **Fig. 8** the *ac*-conductivity as function of both frequency and temperature for the LCBFO compound. As one can see, the *ac*-conductivity is almost constant for low frequency region and increases with increasing temperature. This behavior corresponds to the *dc*-conductivity and confirms the decrease of the resistance with increasing temperature. At high frequency region, the *ac*-conductivity becomes frequency dependent.

The *ac*-conductivity curves were fitted according to the Jonscher's power-low:

$$\sigma_{ac}(\omega,T) = \sigma_{dc} + A \times \omega^{s(T)} \qquad \textbf{Eq. (5)}$$

where σ_{ac}, σ_{dc} and *s* have the known meaning.

The fitted curves for the LCBFO compound are shown in **Fig. 9**.

It was reported that according to the behavior of the $s(T)$, there are four suggested models; Quantum Mechanical Tunneling (QMT) model $(s \approx 0.8)$ **[37]**, Correlated Barrier Jump (CBH) model (s decreases with rising temperature) **[38]**, the Non-overlapping Small Polaron Tunneling (NSPT) (s increases with temperature) **[39]** and the Overlapping Large-Polaron Tunneling (OLPT) model (s decreases and then increases with increasing temperature) **[40]**.

In the present case, the Jonscher's power-low *s* exponent was found to increase when increasing the temperature. We deduced that the *ac*-conductivity obeys the Non-overlapping Small Polaron Tunneling (NSPT) model. According to this model, the exponent temperature dependence of the *s* exponent can be written as:

$$s(T) = 1 + \left(\frac{4 \times k_B}{W_m} \times T\right) \qquad \textbf{Eq. (5)}$$

Where k_B is the Boltzmann's constant and W_m is the binding energy of the carrier in its localized sites. W_m was calculated using the slope of the straight line fitting of the $s(T)$ curve and its value was found to be equal to 80.413 meV (inset of **Fig. 9**).

IV. CONCLUSION

In this work, we have synthesized the $La_{0.72}Ca_{0.18}Bi_{0.1}FeO_3$ (LCBFO) compound by the sol-gel method and performed its structural and morphological characterization by XRD, EDX and TEM. The XRD refinement revealed that the LCBFO compound crystallizes in the orthorhombic structure (*Pnma* space group). TEM image showed a uniform distribution of nanosize grains. The relaxation process and the electrical conductivity are awarded to the same type of charge carriers, which consists in the electrons' jump between iron states. This result is confirmed by the near values of the activation energy determined from both *ac*-conductivity (0.305 eV), the dielectric tangent loss (0.295 eV) and from modulus spectrum (0.298 eV). It has also been found, from the analyses of the Jonscher's power low exponent *s* that the *ac* electrical conduction obeys the NSPT model.

ACKNOWLEDGMENTS

The authors would like to acknowledge the financial support from:

- FCT, Portugal (Project No. UID/CTM/50025/2013 I3N).
- FEDER (Programa Operacional Factores de Competitividade COMPETE)

- FCT-Fundação para a Ciência e a Tecnologia under the Project No. UID/FIS/04564/2016.
- QREN-Mais Centro Project ICT-2009-02-012-1890.

REFERENCES

[1] S. Megahed, W. Ebner, Lithium-ion battery for electronic, J. Power, 54 (1995) 155.

[2] M. Sugimoto, The past, present and future of ferrites, J. Am. Ceram. Soc., 82 (1999) 269.

[3] M. Viret, D. Rubi, D. Colson, D. Lebeugle, A. Forget, P. Bonville, G. Dhalenne, R. Saint-Martin, G. André, F. Ott, β-$NaFeO_2$, a new room-temperature multiferroic material Mater. Res. Bull., 47 (2012) 2294.

[4] J. Suntivich, H.A. Gasteiger, N. Yabuuchi, H. Nakanishi, J.B. Goodenough, S.H. Yang, Design principles for oxygen-reduction activity on perovskite oxide catalysts for fuel cells and metal-air batteries, Nat. Chem. 3 (2011) 546.

[5] B.C. Steele, A. Heinzel, Materials for fuel-cell technologies, Nature 414 (2001) 345.

[6] S. Acharya, J. Mondal, S. Ghosh, S.K. Roy, P.K. Chakrabarti, Multiferroic behavior of lanthanum orthoferrite ($LaFeO_3$), Mater. Lett. 64 (2010) 415.

[7] P. Tirupathi, K. Raju, N. Peetla, R. Pantangi, M. Pastor, Giant dielectric permittivity and weak ferromagnetic behavior in $Bi_{0.5}La_{0.5}Fe_{0.5}Cr_{0.5}O_3$ ceramic, AIP Conference Proceedings, 1731 (2016) 050015.

[8] I.P. Raevski, L. Jastrabik, High dielectric permittivity in non-ferroelectric perovskite ceramics (A=Ba, Sr, Ca; B=Nb, Ta, Sb), J. Appl. Phys., 93, (2003) 4130.

[9] C.-Y. Chung, G.J. Chen, Effects of lanthanum doping on the dielectric properties of ceramic, J. Appl. Phys.,96 (2004) 6624.

[10] C.C. Wang, L.W. Zhang, Dielectric properties of $TbMnO_3$ceramics, Appl. Phys. Lett., 90(2007) 012904.

[11] J. Wu, Y. Deng, Giant dielectric permittivity observed in Li and Ti doped NiO, Phys. Rev. Lett, 89 (2002) 217601.

[12] C. Chen, C.C. Wang, Polaronic relaxation in $LaFeO_3$, Mate. Letters, 89 (2012) 153.

[13] M.H. Hung, M.V.M. Rao, D.S.Tsai, Microstructures and electrical properties of calcium substituted $LaFeO_3$ as SOFC cathode, Mater Chem. Phys., 101 (2007) 297.

[14] L.B. Kong, Y.S. Shen, Gas-sensing property and mechanism of $Ca_xLa_{1-x}FeO_3$ ceramics, Sensor Actuat. B-Chem., 30 (1996) 217.

[15] G. Pecchi, M.G. Jiliberto, A. Buljan, E.J. Delgado,Relation between defects and catalytic activity of calcium doped LaFeO3 perovskite, Solid State Ionics, 187 (2011) 27.

[16] M.A. Alario-Franco, J.M. Gonzalez-Calbet, M. Vallet-Regi, J.C. Grenier, Brownmillerite-type microdomains in the calcium lanthanum ferrites: $Ca_xLa_{1-x}FeO_{3-y}$: (2/3<*x*<1), J. Solid State Chem. 49 (2) (1983) 219.

[17] K.J. Yoon, P.A. Zink, S. Gopalan, U.B. Pal, L.R. Pederson, Defect Chemistry and Electrical Properties of $(La_{0.8}Ca_{0.2})_{0.95}FeO_{3-\delta}$, J. Electrochem. Soc., 156 (2009) B795.

[18] A. Benali, M. Bejar, E. Dhahri, M.F.P. Graça, L.C. Costa, Electrical conductivity and ac dielectric properties of $La_{0.8}Ca_{0.2-x}Pb_xFeO_3$ (*x*=0.05, 0.10 and 0.15) perovskite compounds, J. Alloys ompds., 653 (2015) 506.

[19] A. Benali, A. Souissi, M. Bejar, E. Dhahri, M.F.P. Graca, M.A. Valente, Dielectric properties and alternating current conductivity of sol–gel made $La_{0.8}Ca_{0.2}FeO_3$ compound, Chem. Phys. Letters, 637 (2015) 7.

[20] Z. Shao, G. Xiong, Y. Cong, W. Yang, Synthesis and oxygen permeation study of novel perovskite-type $BaBi_xCo_{0.2}Fe_{0.8-x}O_{3-\delta}$ ceramic membranes, J. Membr. Sci, 164 (2000) 167.

[21] R. Li, Z. Qu, J. Fang, Influence of Bi^{3+} doping on electronic transport properties of $La_{0.5-x}Bi_xCa_{0.5}MnO_3$ manganites, Physica B: Condensed Matter, 406 (2011) 1312.

[22] H. Issaoui, A. Benali, M. Bejar, E. Dhahri, R.F. Santos, N. Kuş, B.A. Nogueira, R. Fausto, B.F.O. Costa, Structural, Morphological, Raman, and Mössbauer Studies on $(La_{0.8}Ca_{0.2})_{1-x}Bi_xFeO_3$ (x = 0.0, 0.1, and 0.2) Compounds, J Supercond. Nov. Magn., (2018) 1-12.

[23] M.A. Ahmed, A.A. Azab, E.H. El-Khawas, Structural, magnetic and electrical properties of Bi doped LaFeO3 nano-crystals, synthesized by auto-combustion method, J. Materials Science: Materials in Electronics, 26 (2015) 8765–8773.

[24] M.P.F. Graça, C. Nico, M. Peres, M.A. Valente, T. Monteiro, J. Nanosci. Nanotechnol, 12 (2012) 1.

[25] M.P.F. Graça, P.R. Prezas, M.M. Costa, M.A. Valente, J. Sol GelSci. Technol. 64 (2012) 78.

[26] R.A. Young, The Rietveld Method, Oxford University Press, New York, 1993.

[27] M.M. Costa, G.F.M. Pires Junior, A.S.B. Sombra, Mater. Chem. Phys. 123 (2010) 35.

[28] A. Guinier, in : X. Dunod (Ed.), Théorie et Technique de la Radiocristallographie, 3rded, (1964) 462.

[29] S. Seto, S. Yamada, K. Suzuki, Structural and optical characterizations of CdTe on CdS grown by hot-wall vacuum evaporation, Solar Energy Mater. Solar Cells, 67 (2001) 167–171.

[30] N. Rezlescu, P.D. Popa, E. Rezlescu, C. Doroftei, Rom. J. Phys., 53 (2008) 545.

[31] Q. Rong, Y.Zhang,T. Lv, K.Shen, B.Zi, Z.Zhu, Q.Liu, Highly selective and sensitive methanol gas sensor based on molecular imprinted silver-doped $LaFeO_3$ core–shell and cage structures. Nanotechnology, 29(14), (2018) 145.

[32] M. Shang, C. Zhang, T. Zhang, L. Yuan, L. Ge, H. Yuan, S. Feng, Appl. Phys. Lett., 102 (2013) 062903.

[33] B. Lal, K.K. Bamzai, P.N. Kotru, B.M. Wanklyn, Mater. Chem. Phys., 2004, 85, 353.

[34] A.S. Mahapatra, A. Mitra, A. Mallick, A. Shaw, J.M. Greneche, P.K. Chakrabarti, Modulation of magnetic and dielectric property of $LaFeO_3$ by simultaneous doping with Ca^{2+} and Co^{2+}-ions, Journal of Alloys and Compounds, 743 (2018) 274.

[35] K. Yoshii, N. Ikeda, A. Nakamura, Magnetic and dielectric properties of frustrated ferrimagnet $TmFe_2O_4$, Physica. B, 585 (2006) 378.

[36] Y. Ma, X.M. Chen, Y.Q. Lin, Relaxor like dielectric behavior and weak ferromagnetism in $YFeO_3$ ceramics, J. Appl. Phys., 103 (2008) 124111.

[37] M. Pollak, Philos. Mag. **23** (1971) 519.

[38] S. Mollah, K.K. Som, K. Bose, B.K. Chaudhuri, J. Appl. Phys. **74** (1993) 931.

[39] A. Ghosh, Phys. Rev. B 41 (1990) 1479.

[40] M. Megdiche, C. Perrin–Pellegrino, M. Gargouri, J. Alloys Compd. 584 (2014) 209.

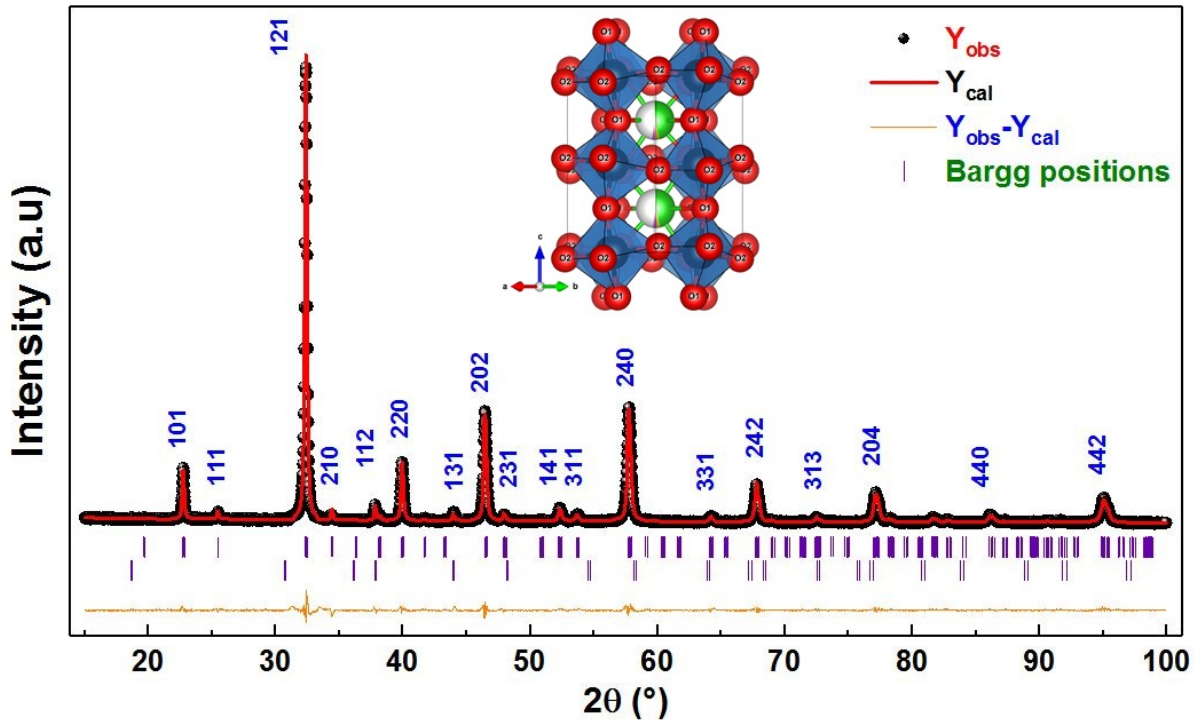

Figure. 1: Rietveld analysis of the X-ray diffraction pattern for $(La_{0.8}Ca_{0.2})_{0.9}Bi_{0.1}FeO_3$ compound.

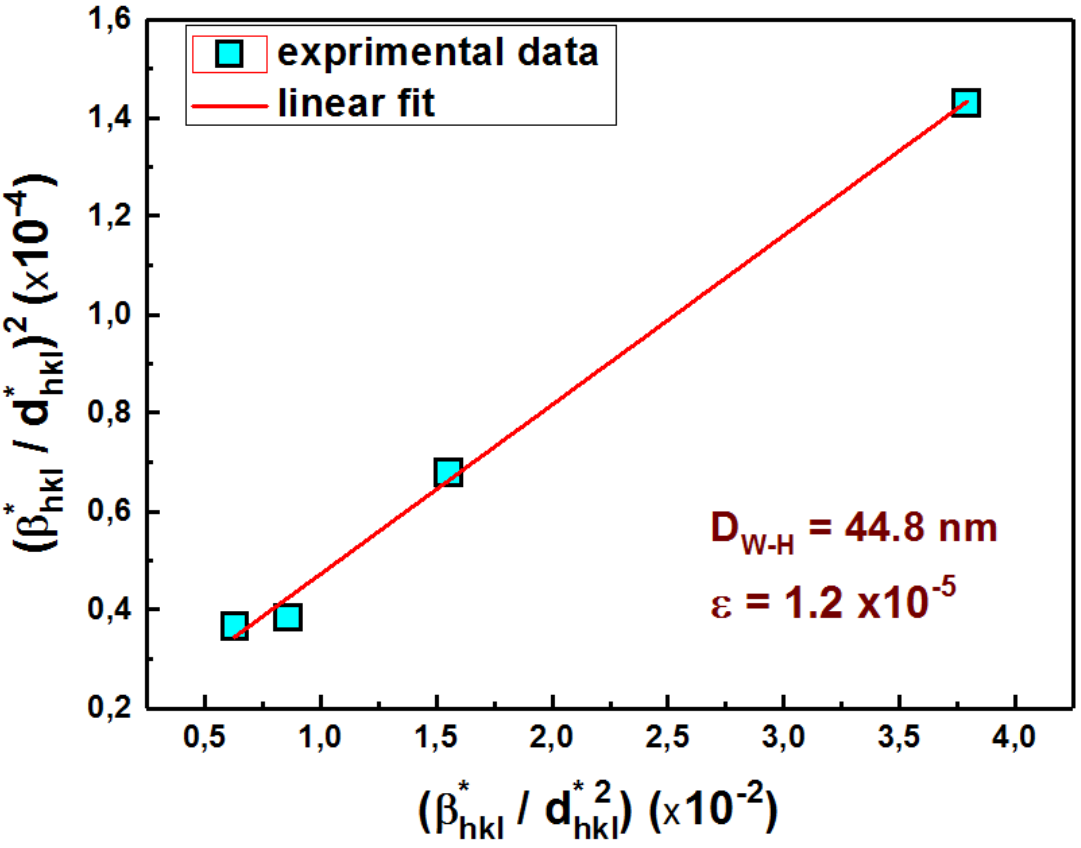

Figure. 2: Halder–Wagner plot of $(La_{0.8}Ca_{0.2})_{0.9}Bi_{0.1}FeO_3$ compound.

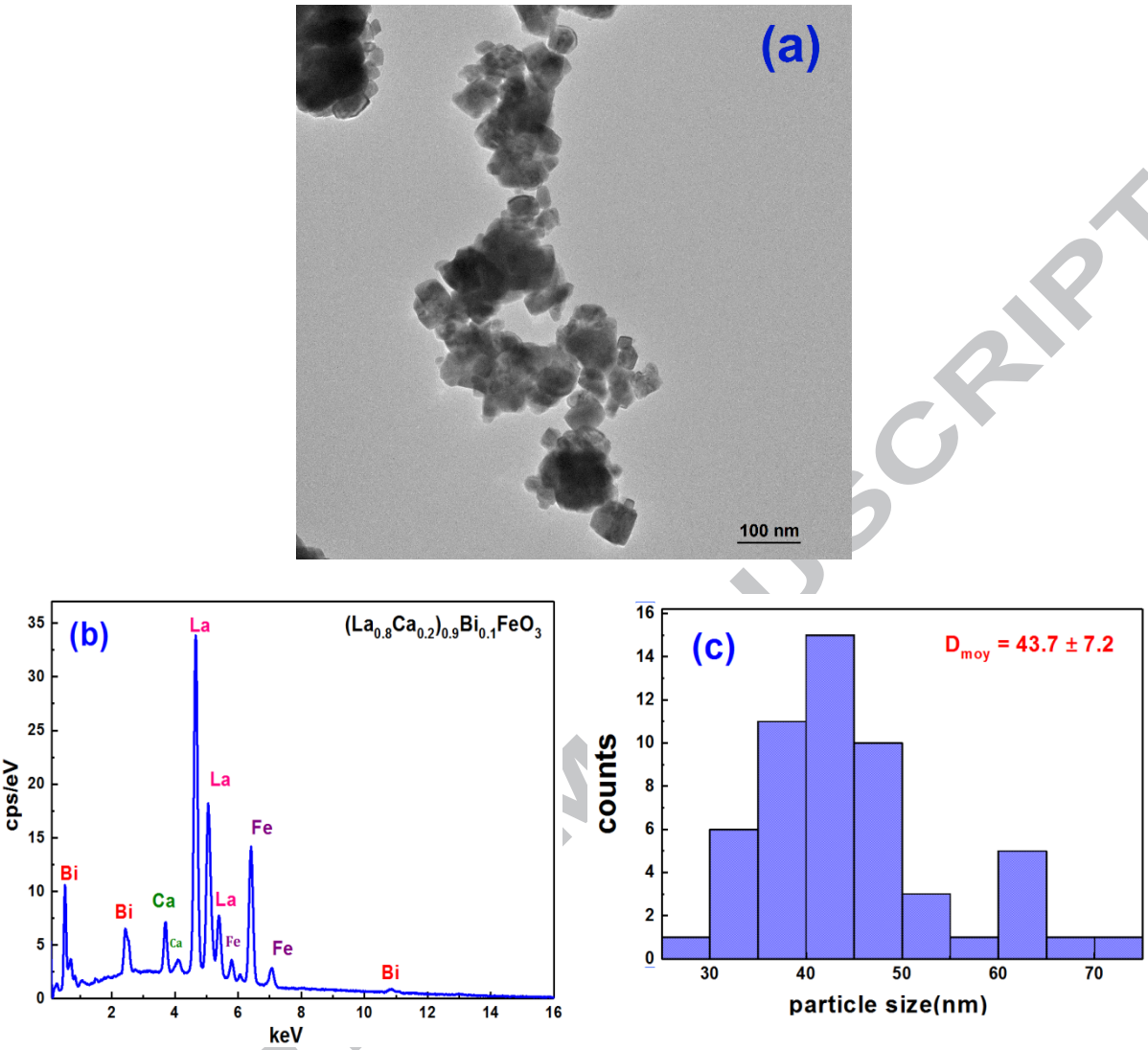

Figure. 3: (***a***) SEM image, (***b***) EDX analysis, **(c)** particle size distribution of $(La_{0.8}Ca_{0.2})_{0.9}Bi_{0.1}FeO_3$ compound.

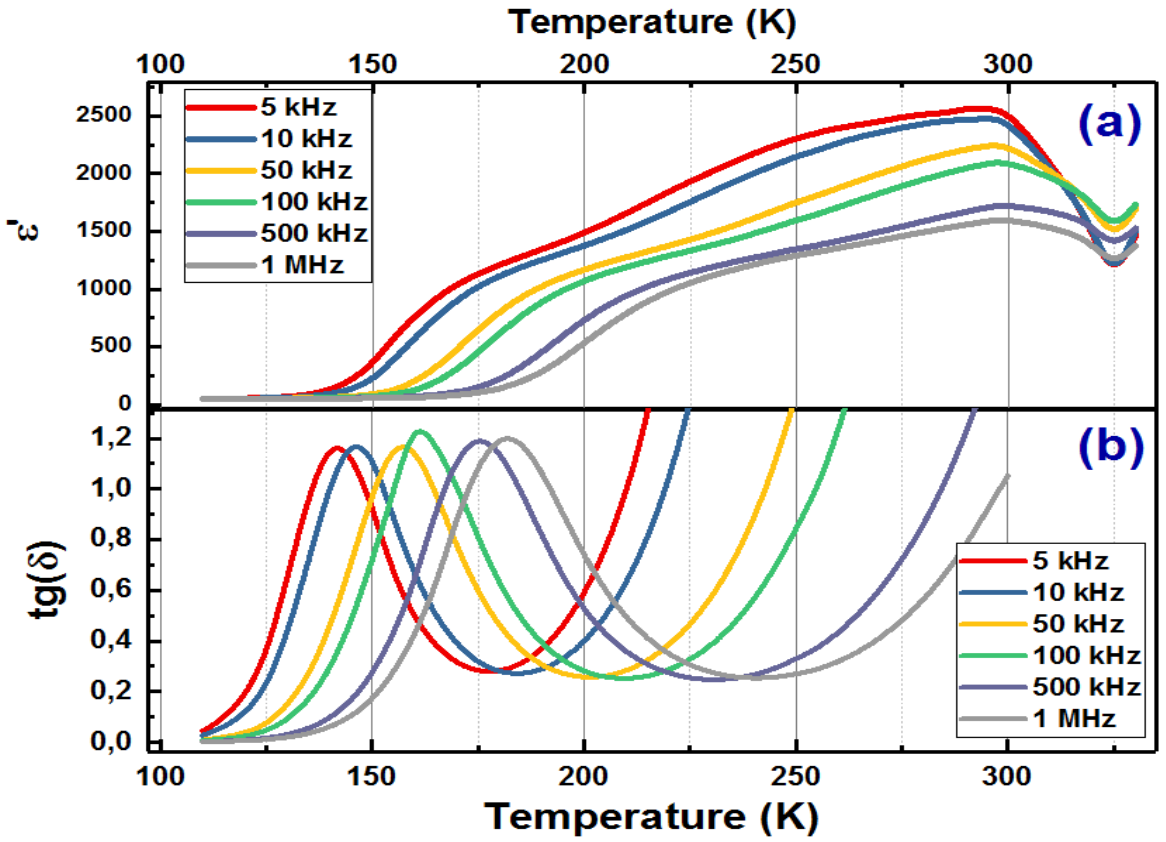

Figure. 4: The temperature dependence of the dielectric constant (ε') **(*a*)** and the dielectric loss $(tg\delta)$ **(*b*)** at several frequencies of $(La_{0.8}Ca_{0.2})_{0.9}Bi_{0.1}FeO_3$ compound.

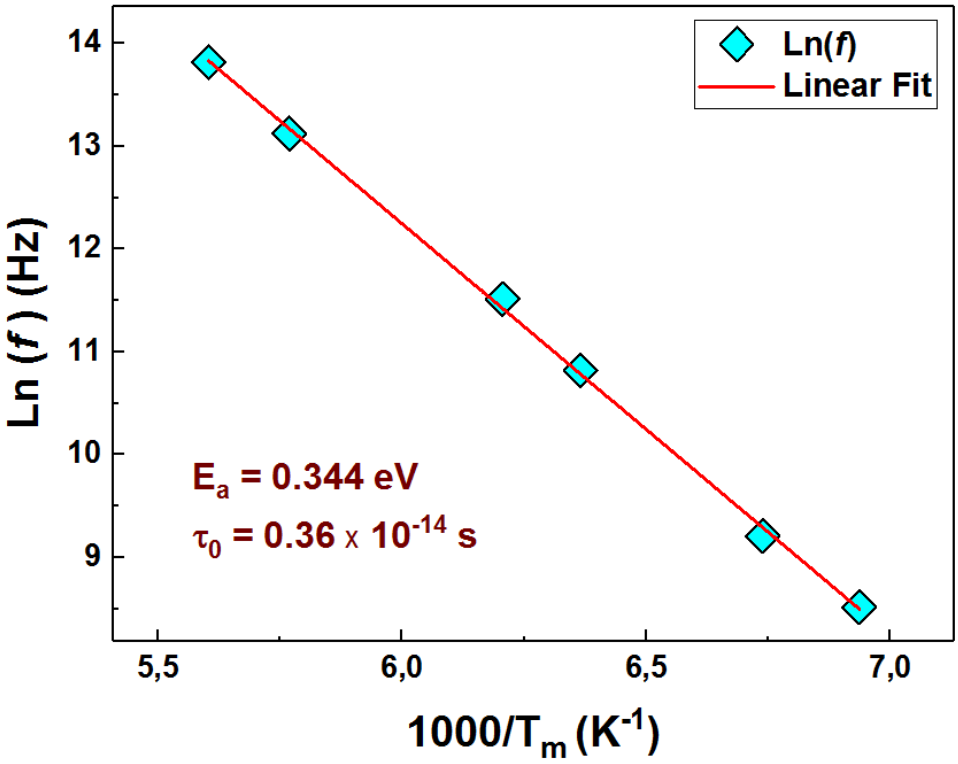

Figure. 5: Variation of ***Ln(f)*** as function of **1000/T_m** of $(La_{0.8}Ca_{0.2})_{0.9}Bi_{0.1}FeO_3$ compound.

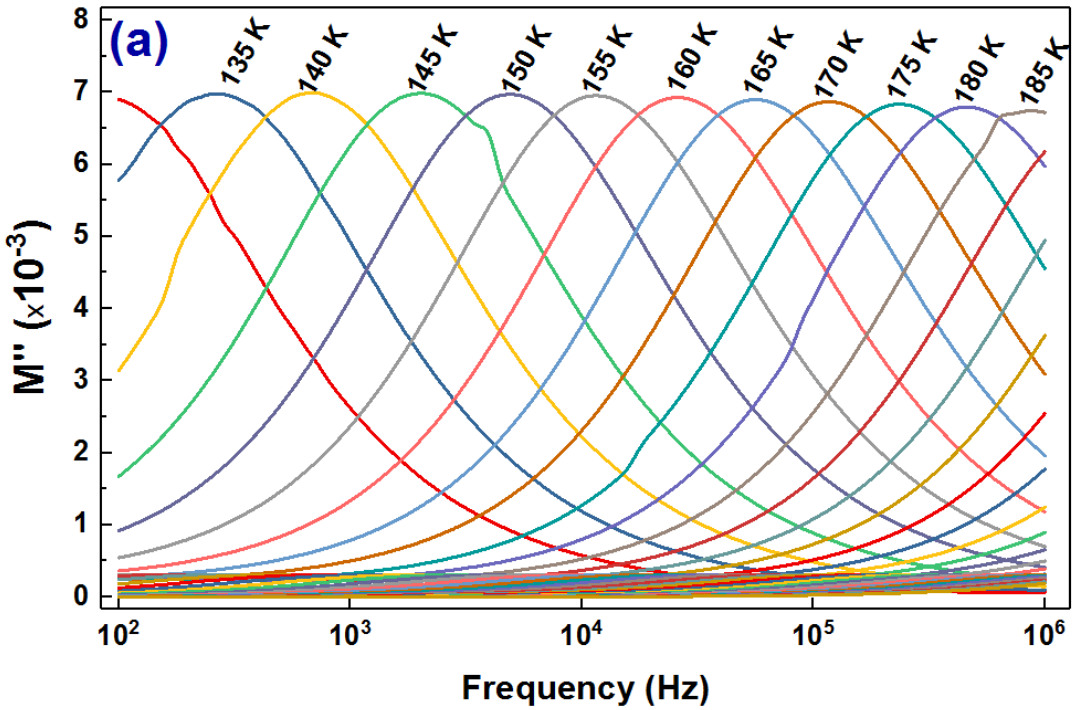

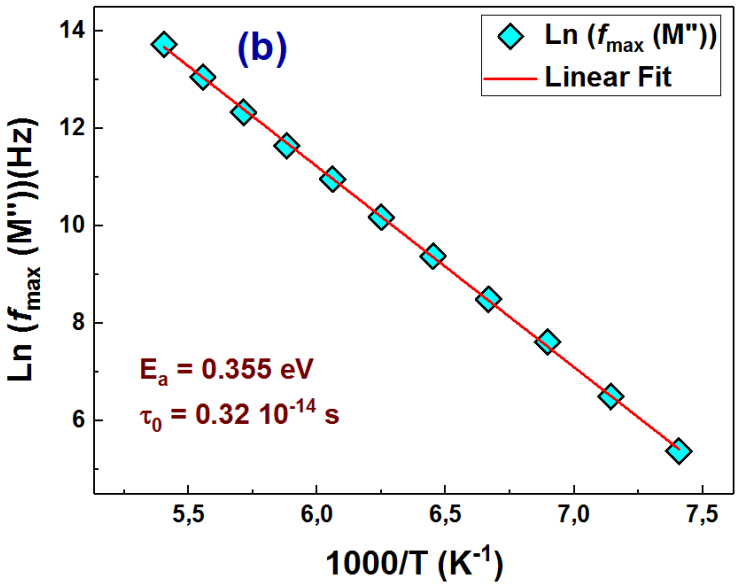

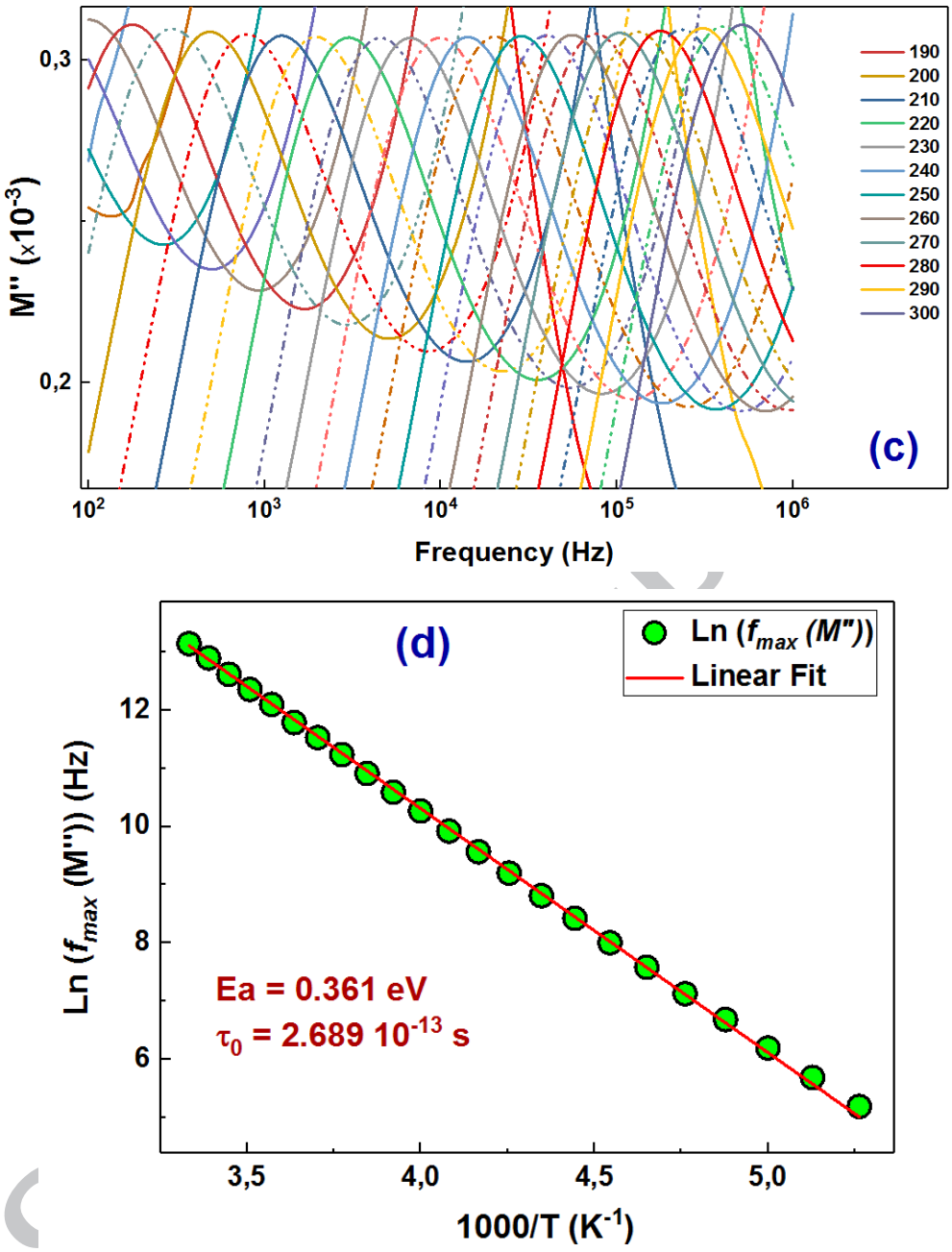

Figure. 6: **(a)** and **(c)** frequency dependence of the imaginary part of the Modulus (M") correspondent to grains and boundary grains relaxations, respectively **(b)** and **(d)** the Arrhenius plots for both relaxations (inset the corresponding activation energy and the relaxation time values).

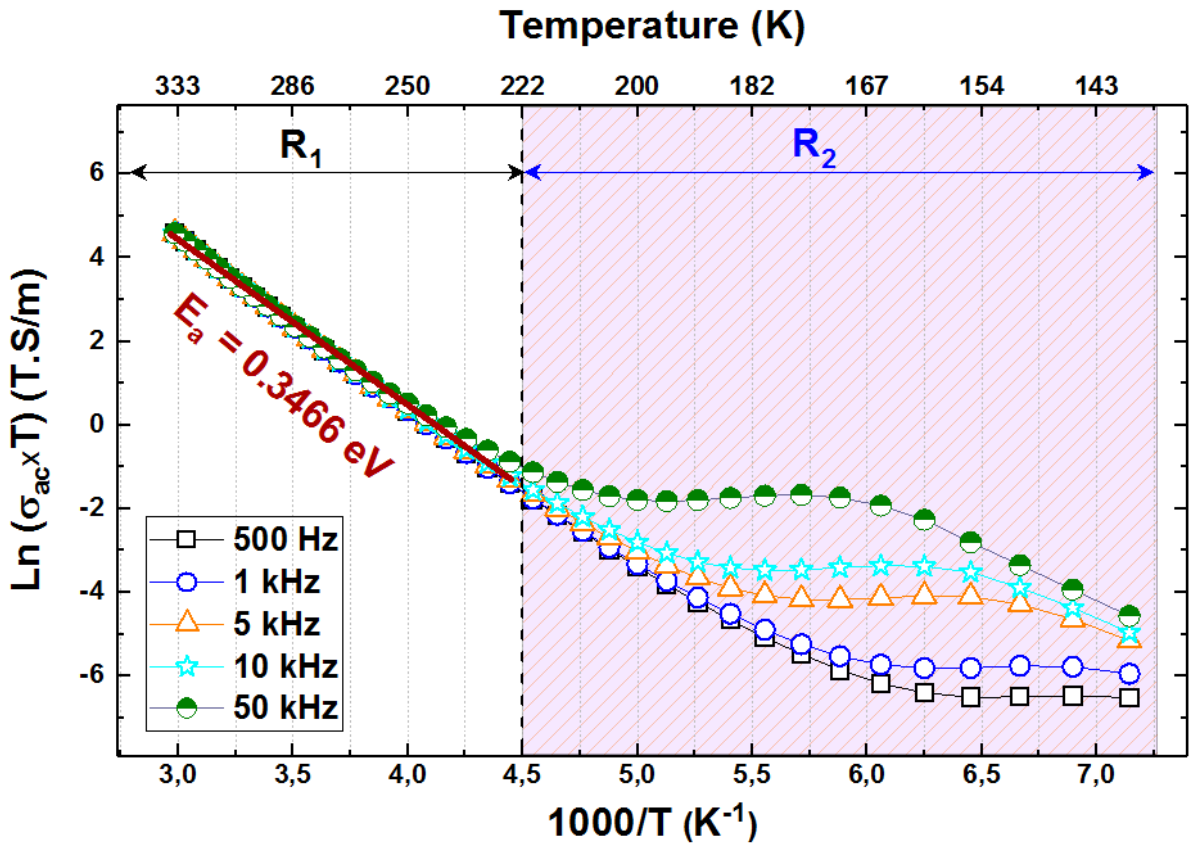

Figure. 7: Variation **Ln (σ_{ac} x T)** of as a function of **1000/T_m** of $(La_{0.8}Ca_{0.2})_{0.9}Bi_{0.1}FeO_3$ compound.

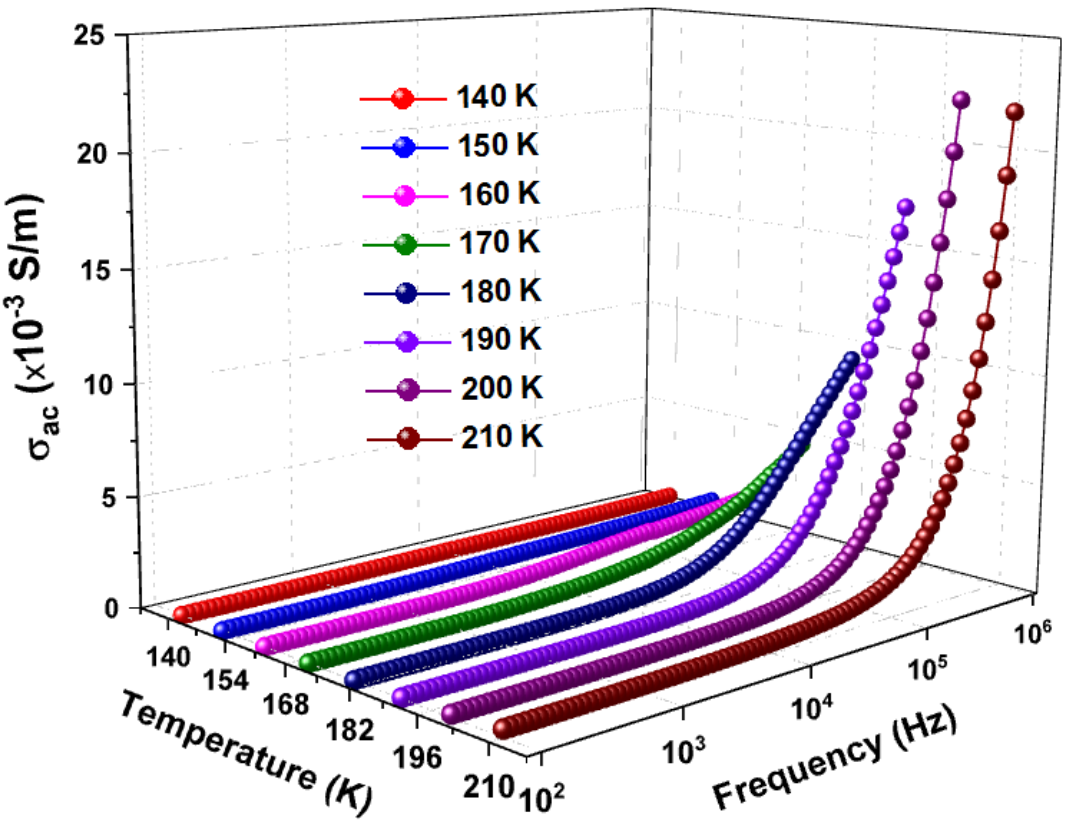

Figure. 8: Variation of the *ac*-conductivity σ_{ac} as a function of both frequency and temperature of $(La_{0.8}Ca_{0.2})_{0.9}Bi_{0.1}FeO_3$ compound.

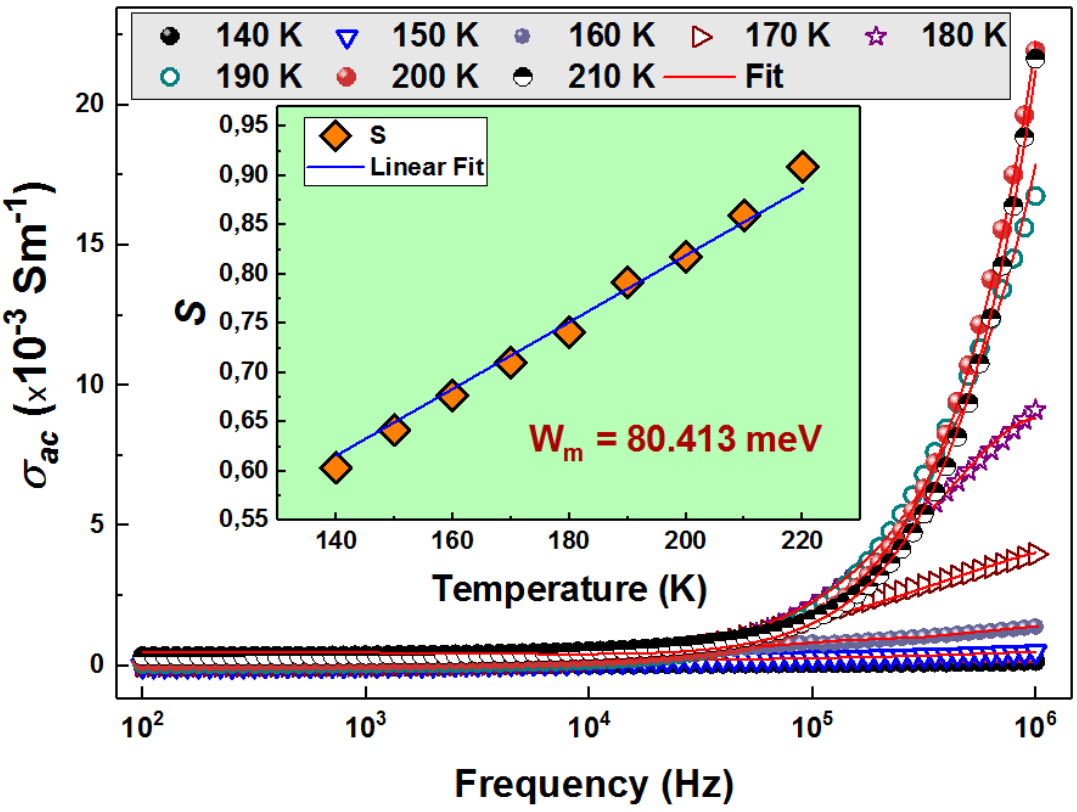

Figure. 9: Variation of the *ac*-conductivity σ_{ac} as a function of frequency and of the *s* exponent as a function of temperature of $(La_{0.8}Ca_{0.2})_{0.9}Bi_{0.1}FeO_3$ compound.

Table 1: Rietveld refinement results of the $(La_{0.8}Ca_{0.2})_{0.9}Bi_{0.1}FeO_3$ compound.

a (Å)	b (Å)	c (Å)	Fe-O_1 (Å)
5.513(6)	7.797(2)	5.527(6)	1.96483(5)
Fe-O_2 (Å)	**Fe-O_1-Fe (°)**	**Fe-O_2-Fe (°)**	
2.11114(6)	159.748(6)	151.611(6)	

RESEARCH HIGHLIGHTS

- $(La_{0.8}Ca_{0.2})_{0.9}Bi_{0.1}FeO_3$ (LCBFO) compound was synthesized by the sol-gel method using the citric acid route and crystallized in the orthorhombic structure with the (Pbnm) space group
- The TEM confirmed the nanosize of particles.
- The modulus formalism indicating the presence of a single relaxation peak.
- The activation energy values obtained from both ac conductivity, the tang (δ) spectrum and from modulus spectrum are found to be very similar.
- The activation energy was calculated from the ac-conductivity, the dielectric loss tangent, the dielectric constant and from the imaginary part of Modulus. All values are very close and confirmed the polaronic relaxation.
- The electrical conductivity curves obeying to the Jonscher's universal power law where the S parameter behaviour confirmed that the NSPT model is the suitable one to analyse the ac-conductivity.

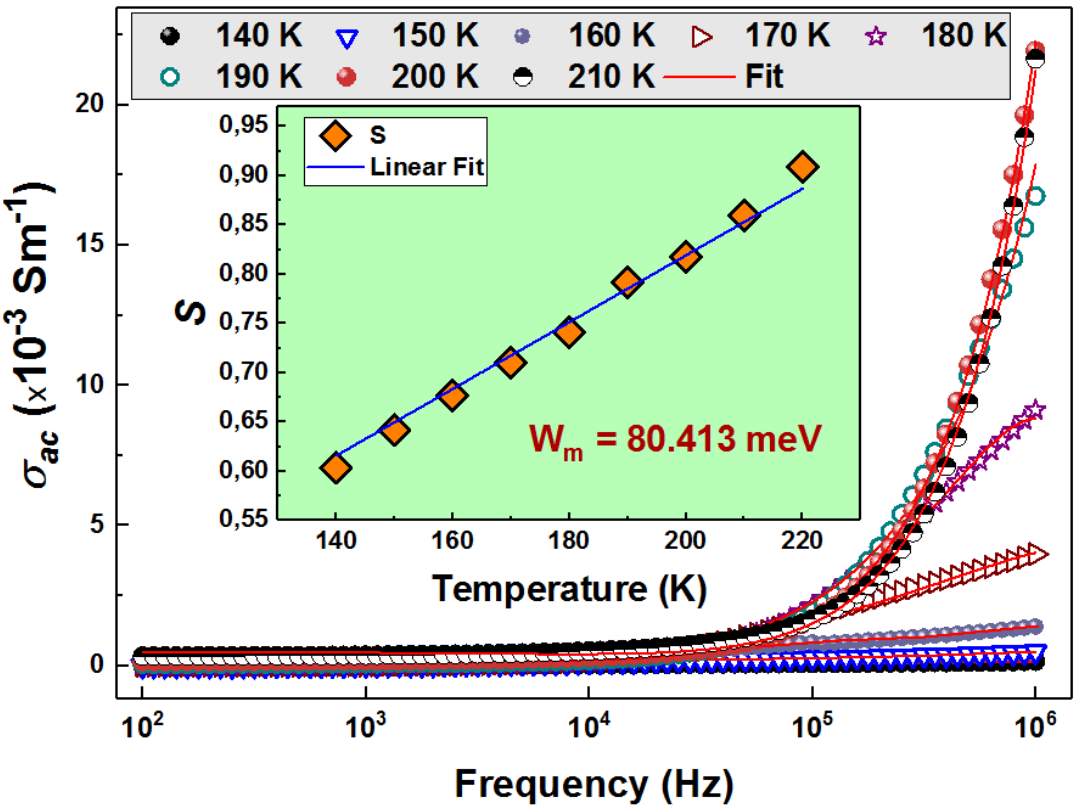

Variation of the *ac*-conductivity (σ_{ac}) as a function of frequency and of the *s* exponent as a function of temperature of $(La_{0.8}Ca_{0.2})_{0.9}Bi_{0.1}FeO_3$ compound.

DECLARATION OF INTEREST STATEMENT

The present work investigates the structural, morphological, dielectric and electric properties of the multiferroic $(La_{0.8}Ca_{0.2})_{0.9}Bi_{0.1}FeO_3$ compound. The dielectric properties were found to be strongly dependent on both temperature and frequency. A relaxation was shown in the imaginary part of the modulus (M”), in the dielectric tangent loss tg(δ) and in the dielectric constant curves. From the calculated activation energies from all parameters we assign the relaxation process to be polaronic.

In addition, the analysis of the frequency-dependent of the ac-conductivity revealed that then non-overlapping small polaron (NSPT) is the most appropriate model of conduction into the prepared compound.